Diffuse Galactic Gamma Rays at intermediate and high Latitudes, Constraints on ISM properties

Maryam Tavakoli
I.Cholis, C.Evoli, P.Ullio
SISSA & INFN, Trieste; National Astronomical Observatory of China
tavakoli@sissa.it, ilias.cholis@sissa.it, carmelo.evoli@me.com, ullio@sissa.it

Abstract

Recently published γ-ray spectral data from the Fermi Collaboration have provided the possibility to study the diffuse γ-ray sky at medium and high latitudes ($\mid b \mid > 10^{\circ}$) and energies of 1-100 GeV with unprecedented accuracy. This gives us the chance of analyzing the properties of sources and propagation of cosmic rays (CRs) in the Galaxy. Implementing the publicly available DRAGON code, we have performed a detailed study on assumptions done in the literature for the interstellar HI and H2 gas distributions, as well as tests on a variety of propagation models. Each model assumes a distinct global profile for the diffusion and the re-acceleration of CRs. Fitting propagation parameters to well measured local CRs such as, the B/C ratio, p, $\bar{p}$ and $e^{\pm}$ fluxes, we evaluate the γ-ray spectra at medium and high latitudes in order to place further constraints on these models of propagation.

1. Introduction

Interactions of CRs with the interstellar medium (ISM) are a copius source of gamma rays. Inelastic collisions of CR protons and helium with interstellar gas (ISG) produce π^0s which subsequently decay into 2 photons. Photons produced in this process constitute the main contribution to the diffuse gamma ray flux from the Milky Way in the intermediate GeV range and trace the ISG target distribution dominated by the HI and H2 gasses. Bremsstrahlung off CR $e^{\pm}$ in the ISG and the inverse Compton scattering (ICS) of CR $e^{\pm}$ off the interstellar radiation field (ISRF) and the CMB are the two other mechanisms which dominantly produce diffuse galactic γ-rays at least up to energies ~ 100 GeV. Apart from diffuse galactic γ-rays, the observed fluxes include galactic and extragalactic point sources [1] as well as isotropic components of extragalactic and instrumental origin. Thus a detailed study of different models for CR propagation, CR sources, ISG, ISRF and galactic magnetic fields is crucial for studying the γ-ray spectrum.

The propagation of CRs in the Galaxy at energies below 10^{17} eV can be described by:

$$\frac{\partial \psi(\vec{r},p,t)}{\partial t} = q(\vec{r},p,t) + \vec{\nabla}.(D_{xx}\vec{\nabla}\psi) + \frac{\partial}{\partial p}\Big[p^2 D_{pp}\frac{\partial}{\partial p}(\frac{\psi}{p^2})\Big] - \frac{\partial}{\partial p}(\dot{p}\psi) - \vec{\nabla}.(\vec{V}\psi) + \frac{\partial}{\partial p}\Big[\frac{p}{3}(\vec{\nabla}.\vec{V})\psi\Big] - \frac{\psi}{\tau_{frag}} - \frac{\psi}{\tau_{decay}} \quad (1)$$

where $\psi(\vec{r},p,t)$ is the density per unit particle momentum, $q(\vec{r},p,t)$ is the source term including components of primary origin, as well as CRs from spallation and decay processes, $D_{xx}(\vec{r})$ and $D_{pp}(\vec{r})$ are the diffusion tensors in, respectively, the position and momentum space, $\dot{p}$ is the momentum loss rate due to interactions with interstellar medium (ISM), the Galactic magnetic field or the ISRF, $\vec{V}$ is the convection velocity (consistently with the literature we put $\vec{V}=0$), and τ_{frag} and τ_{decay} are the timescales for, respectively, fragmentation loss and radioactive decay.

For our simulations we use the DRAGON code [2] which solves numerically Eq. (1) in a 3D grid: 2 spatial dimensions for galactocentric radial distance $r\epsilon(0,20)(kpc)$ and height from the galactic plane $z\epsilon(-20,20)(kpc)$, and 1 for the momentum p.

2. Assumptions

Primary Sources: CR primary sources up to energies of $\sim$ 100TeV, are supernova remnants (SNRs). For each nucleus i the source term describing the injection of CRs in the ISM is given as a function of rigidity, R, by:

$$q_i(r,z,E) = f_s(r,z) q_{0,i} (\frac{R(E)}{R_0})^{-\gamma_i}\,, \quad (2)$$

where $q_{0,i}$ is the normalization of the injected CR species, $f_s(r,z)$ traces the distribution of SNRs as modeled in [3] on the basis of pulsar and progenitor star surveys [4].

Electrons and positrons accelerated between a pulsar and the termination shock of the wind nebula, may also contribute to the high energy $e^{\pm}$ spectrum, and then to the γ-ray flux. Each pulsar contribution to the $e^{\pm}$ fluxes can be described by an injection spectrum $\sim E^{-n}$ with a high energy break E_b estimated at the time the surrounding pulsar wind nebula (PWD) is disrupted leading to the $e^{\pm}$ escaping into the ISM. We fit the properties of a pulsar distribution following the parametrization of [5]:

$$Q_p(r,z,t,E) = J_0 E^{-n} e^{-E/M} f_p(r,z)\,, \quad (3)$$

where M is a statistical cut-off, n the injection index for the distribution of pulsars and $f_p(r,z)$ describes the spatial distribution of young pulsars in the Galaxy as given in[6].

Magnetic fields and Diffusion: The large scale galactic magnetic field is generally assumed to be a bi-symmetrical spiral with a small pitch angle [7]. Here we assume that the regular magnetic field is purely azimuthal, $\vec{B_0} = B_0\hat{\phi}$, and has the form

$$B_0 = 3\exp(-\frac{r-r_{\odot}}{11(kpc)})\exp(-\frac{|z|}{2(kpc)})(\mu\mathrm{G}) \quad (4)$$

based on the analysis of WMAP synchrotron intensity and polarization data in [8]. As the B-field decreases moving away from the galactic center, the diffusion coefficient is expected to increase at large r and z. On the basis of [2] for vertical profile, we choose the spatial part of D to be proportional to some negative power of large scale galactic magnetic field. Thus, assuming isotropic diffusion, the diffusion coefficient in CR transport equation can be modeled as:

$$D(r,z,R) = D_0\beta^{\eta}(\frac{R}{R_0})^{\delta}\exp(\frac{r-r_{\odot}}{r_d})\exp(\frac{|z|}{z_d})\,, \quad (5)$$

where $R_0 = 3GV$ is the reference rigidity and δ is the diffusion spectral index which is related to different ISM turbulence power-spectrum. The dependence of diffusion on the particle velocity, $\beta = v_p/c$, is naturally expected to be linear ($\eta = 1$), however the analysis by [9] shows an increase in diffusion at low energies. To represent such a behavior, the parameter η has been introduced by [10].

Interstellar Gas: The interstellar gas is composed of hydrogen, helium and small contributions from heavier elements, with hydrogen observed in atomic (HI), molecular (H2) and ionized (HII) states.

The three dimensional distribution of HI gas can be derived from 21-cm spectra information and rotation curves. The model which has been widely used in the literature is developed by [11, 12], while we use as a reference the model developed by [13].

Molecular hydrogen can exist only in dark cool clouds where it is protected against the ionizing stellar ultraviolet radiation. It can be traced with the λ = 2.6 mm (J = 1 $\rightarrow$ 0) emission line of CO, since collisions between the CO and H2 molecules in the clouds are responsible for the excitation of CO. The CO to H2 conversion factor, X_{CO} which relates the H2 column density, N_{H2} , to the velocity-integrated intensity of the CO line, through $N_{H2} = X_{CO}T_bV_r$, has considerable uncertainties. For this reason we study different HI and H2 three-dimensional distribution models as shown in Fig. 1, where we present the radial and vertical profiles of HI and H2 volume density among the different models. For the H2 distribution we use for our reference model the map provided by [14], assuming the conversion factor to vary exponentially with galactocentric radius:

$$X_{CO}[H_2 cm^{-2} K^{-1} km^{-1} s] = 1.4\exp(\frac{R}{11(kpc)}), \quad (6)$$

however [15] is also an older widely used model in the literature.

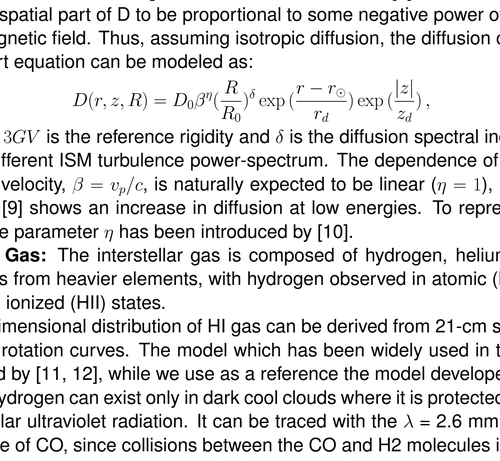

Figure 1: *Large scale density distributions of atomic and molecular hydrogen in the Galaxy vs r for $z = 0$(*left*); vs z for $r = r_{\odot}$ (*right*).*

Ionized hydrogen occurs in the vicinity of young O and B stars, with the ultraviolet radiation from these stars ionizing the ISM. HII regions have a similar distribution to the molecular hydrogen, but mass-wise their contribution is negligible. Thus we choose not to vary the averaged large-scale distribution of this gas component.

Finally Helium appears to follow the hydrogen distribution with a factor $He/H = 0.10 \pm 0.08$. We adopt a value of $He/H = 0.11$, which is widely used in the literature, and neglect heavier nuclear species.

3. Analysis

We consider a range of values for the height and radial scales of the diffusion coefficient, z_d and r_d, as well as for the diffusion index δ in Eq. (5). For each set of values of δ, z_d and r_d, we sample the parameter space (D_0, η, v_A) by minimizing the χ^2 for B/C data (see Fig. 2 (upper left)). We then fix the spectral properties of the CR protons as shown in Fig. 2 (upper right), while checking also the consistency of the predicted antiproton flux with local measurements (Fig. 2 (lower left)).

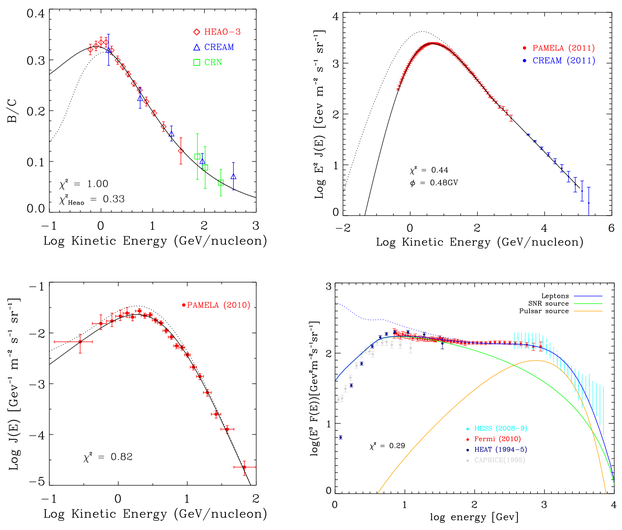

Figure 2: *Reference model. We assume that $D = D_0\beta^{\eta}(R/3GV)^{0.5}e^{|z|/4}e^{(r-r_{\odot})/20}$ (where R is the rigidity) as in Eq. (5).* Upper left*: fit to the B/C data setting $D_0 = 2.49\times10^{28}cm^2s^{-1}$, $\eta = -0.363$ and $v_A = 19.5kms^{-1}$.* Upper right*: the local proton flux - the PAMELA and CREAM data are used to fit the proton source function.* Lower left*: the predicted antiproton spectrum provides a good fit to the PAMELA data.* Lower right*: the measured $e^+ + e^-$ flux sets constraints on the primary, secondary and pulsar components - the fit to the data gives $n = 1.4$, $M = 1.2$ TeV and $\overline{\eta W_0} \simeq 10^{49}$ erg per pulsar, well within the allowed range of values.*

He and heavier CR nuclei spectral assumptions are also checked for consistency with the most recent data. Since the electron flux below $E \sim 30$ GeV, is dominated by SNe accelerated electrons(primaries) and secondary electrons (and positrons) from inelastic collisions of CR nuclei with the ISM, we fit the primary and secondary electrons spectral properties to the $e^+ + e^-$ spectrum between 7-30 GeV as measured by *Fermi* . Pulsars within $\sim$ 3kpc can contribute to the $e^+ + e^-$ spectrum up to $O(0.1)$ at $E \approx 50$ GeV and up to $O(1)$ at $E \approx 500$ GeV. Thus assuming pulsars contribute maximally, we find from the *Fermi* data the injection index n for the distribution of pulsars of Eq. 3 and the averaged total energy injected into the ISM through CR $e^{\pm}$ per pulsar ηW_0 (Figure 2(lower right)). Note that, for consistency, we compare as well against the *PAMELA* positron fraction and the recently released electrons only spectrum. Having fixed all the properties of the CR electrons from SNe and pulsars we then calculate the γ-ray diffuse spectra.

4. Results

As reference model providing a good combined fit of the local CRs (see Fig. 2) and the γ-rays at intermediate and high latitudes (Fig. 3), we have implemented model "KRA4_20" which has: $\delta = 0.5$, $z_d = 4$ kpc, $r_d = 20$ kpc. A very good fit to the γ-ray spectrum is achieved at the highest latitudes ($\mid b \mid > 60^{\circ}$), the range less affected by uncertainties in the sources distribution [16]. We note that the "source" components that we show are the sources detected with at least 14 σ and also weaker sources that have been catalogued by LAT [1]. Yet very dim γ-ray sources that would be contributing per energy bin and pixel less photons than the uncertainty on the true diffuse background are not included. Such a class of sources could be millisecond pulsars (MSPs) in the galactic ridge and halo that are not modeled for. Such MSPs that are not in globular clusters can contribute in the lower latitudes and could possibly compensate for our under-prediction of the total gamma-ray flux at $\sim$ few GeV.

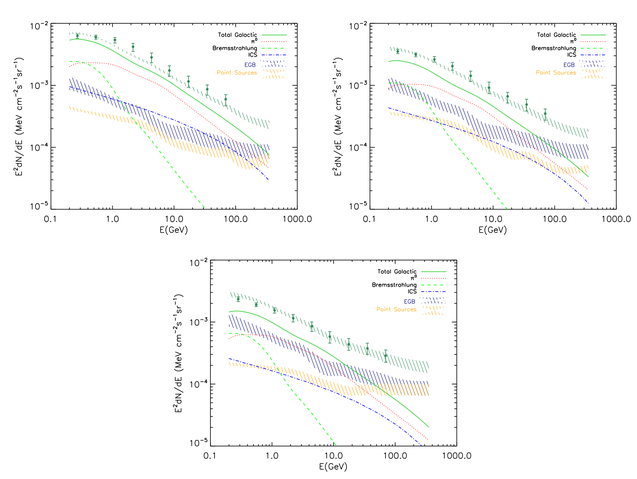

Figure 3: *Reference model, predictions for the γ-ray flux, see text and Fig. 2 for more details.* Upper left*: $10^{\circ} < \mid b \mid < 20^{\circ}$ and $0^{\circ} < \mid l \mid < 360^{\circ}$,* upper right*: $20^{\circ} < \mid b \mid < 60^{\circ}$ and $0^{\circ} < \mid l \mid < 360^{\circ}$,* lower*: $60^{\circ} < \mid b \mid < 90^{\circ}$ and $0^{\circ} < \mid l \mid < 360^{\circ}$.*

In Fig. 4 we plot the γ-ray spectra at the three latitude regions of study when varying the diffusion index. The π^0 component depend on the proton spectra scaling in turn with the diffusion timescale. Lower values of the diffusion index δ make the protons propagated spectra harder, resulting in the need for a softer proton injection index as shown in Table 1. In fact since we fit to the PAMELA and CREAM data, it is the difference in the injection indices below 300 GeV that causes the differences in the π^0 fluxes. Unlike protons, electrons propagation with energies above 5 GeV is mainly affected by the energy loss time-scale and, since the ISRF and B-field model are kept fixed, the ICS and the higher part of the bremsstrahlung spectrum are not affected much. At the very high energy part of the ICS spectrum we see though the expected hardening of the models with greater δ. On the lower energy part of the spectrum where bremsstrahlung varies significantly among the models the reason for those differences is related to the very different Alfven velocities used (in order to fit the CR data). We notice that the overall fit of the gamma-ray spectra is not affected much due to opposite effects of changing the value of δ on the bremsstrahlung and π^0 lower parts of their spectra.

Figure 4: *Predictions for a few values of the diffusion index δ; plots refer to the different sky regions of our study.* dotted lines*: $\delta = 0.5$,* dashed lines*: $\delta = 0.4$,* dashed-dotted lines*: $\delta = 0.33$. For all $z_d = 4$ kpc and $r_d = 20$ kpc.*

In Fig. 5 we vary the radial scale for the diffusion coefficient r_d. Decreasing the value of r_d results in lower values for the diffusion coefficient towards the Galactic center, which forces the $e^{\pm}$ and p produced by sources closer to the Galactic center to spend greater time close to the disk. Since we refit, based on the B/C flux ratio, the diffusion coefficient D_0 (see Table 1), the net change in the fluxes is negligible.

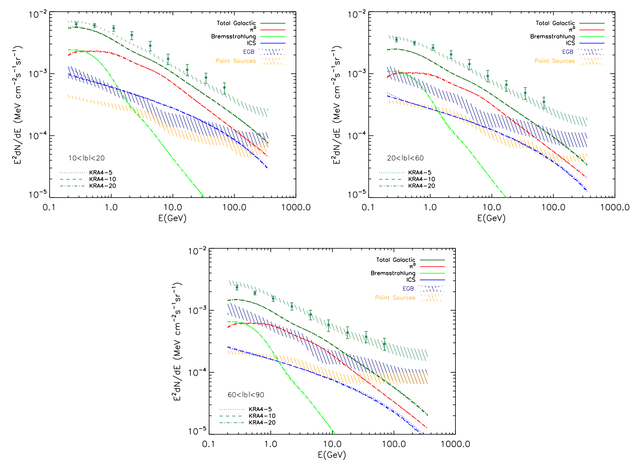

Figure 5: *Predictions varying the diffusion radial scale r_d; plots refer to the different sky regions of our study.* dotted lines*: $r_d = 5$ kpc,* dashed lines*: $r_d = 10$ kpc,* dashed-dotted lines*: $r_d = 20$ kpc. For all $\delta = 0.5$ and $z_d = 4$ kpc.*

Name	δ	z_d	r_d	D_0	v_A	η	γ_1^p	$Br_1(GV)$	γ_2^p	$Br_2(GV)$	γ_3^p
KRA4-5	0.5	4	5	2.76	16.9	0.0	2.05	25	2.34	300	2.18
KRA4-10	0.5	4	10	2.58	19.1	-0.247	2.05	20	2.34	300	2.18
KRA4-20	0.5	4	20	2.49	19.5	-0.363	2.05	15	2.34	300	2.18
RUN4-20	0.4	4	20	3.21	23.15	0.32	2.05	12	2.4	300	2.27
KOL4-20	0.33	4	20	3.85	24.82	0.765	2.07	10	2.48	300	2.34

Table 1: *The parameters for the various models of propagation. See text, γ_1^p is the protons injection index below the Br_1, γ_2^p the injection index between Br_1 and Br_2, and γ_3^p above Br_2. For primary electrons we assumed one break at 5 GV above(below) which, the injection index is 2.62(1.6).*

References

[1] Abdo et al. 2010 Phys. Rev. Lett. *104*, 101101.

[2] Evoli C., Gaggero D., Grasso L., & Maccione L. 2008 JCAP *10*, 018

[3] Ferriere K. M. 2001 Rev.Mod.Phys. *73*, 1031

[4] Evoli C., Grasso L., & Maccione L. 2007 JCAP *0706*, 003

[5] Malyshev D., Cholis I., & Gelfand J. 2009 Phys.Rev. *D80*, 063005

[6] Faucher-Giguere C.-A., & Kaspi V. M. 2006 ApJ *643*, 332

[7] Jansson R., Farrar G. R., Waelkens A. H., & Ensslin T. A. 2009 JCAP *0907*, 021

[8] Miville-Deschenes et al. arXiv:0802.3345

[9] Ptuskin et al. 2006 ApJ *642*, 902

[10] Di Bernardo G., Evoli C., Gaggero D., Grasso L., & Maccione L. 2010 arXiv:1010.0174

[11] Gordon M. A., & Burton W. B. 1976 ApJ *208*, 346

[12] Dickey J. M., & Lockman F. J. 1990 A&A *28*, 215

[13] Nakanishi H., & Sofue Y. 2003 Publ. Astron. Soc. Jap. *53*, 191

[14] Nakanishi H., & Sofue Y. arXiv:astro-ph/0610769

[15] Bronfman L., Cohen R. S., Alvarez H., May J., & Thaddeus P. 1988 ApJ *324*, 248

[16] Cholis I., Evoli C., Tavakoli M, & Ullio P. in preperation